agreement with Avrami exponent values. Conventional interpretations would ascribe the change in Avrami exponent from 4 to 3 as reflecting a change in nucleation patterns from sporadic to instantaneous. Such an observation is consistent with earlier comments on $t_{1/2}$ analyses which suggested a greater sporadic component at atmospheric pressure. In the axialitic region, detailed interpretation is difficult at this time. A change from 3 to 2 using theoretical models could be interpreted as a change from sporadic disk to instantaneous disk morphologies or a change from instantaneous sphere to instantaneous disk. The disk models might seem more appropriate for axialites; however, the situation is complicated because of the molecular weight distribution and the likely crystallization of the higher molecular weight fractions as regime II at all temperatures. Resolution of this problem must await detailed morphological evaluation together with studies on sharp fractions.

Conclusions

Pressure dependence of the fold surface free energy of the critical nucleus of polyethylene is consistent with the tightly folded adjacent reentry model over the range of pressures studied. Bulk kinetic studies can detect the presence of regime transitions when analyzed by a Lauritzen–Hoffman approach if the mode of nucleation is predominantly instantaneous in nature. Estimation of fold surface free energies using bulk kinetic data depends very much on the nucleation characteristics of the specimen being studied.

Acknowledgment. This research has been supported by the National Science Foundation, Polymers Program, under Grants DMR-8320212 and DMR-8106033.

Registry No. Sclair 2907, 9002-88-4.

References and Notes

(1) B. Wunderlich and T. Arakawa, *J. Polym. Sci., Part A*, **2**, 3697 (1964).
(2) B. Wunderlich and L. Melillo, *Makromol. Chem.*, 118 250 (1968).
(3) R. B. Prime and B. Wunderlich, *J. Polym. Sci., Part A-2*, **7**, 2061 (1969).
(4) D. V. Rees and D. C. Bassett, *J. Polym. Sci., Part A-2*, **9**, 385 (1971).
(5) D. C. Bassett and B. Turner, *Nature (London), Phys. Sci.*, **240**, 146 (1972).
(6) D. C. Bassett, S. Block, and G. J. Piermarini, *J. Appl. Phys.*, **45**, 4146 (1974).
(7) D. C. Bassett, *Polymer*, **17**, 460 (1976).
(8) J. I. Lauritzen and J. D. Hoffman, *J. Appl. Phys.* **44**, 4340 (1973).
(9) J. D. Hoffman, G. T. Davis, and J. I. Lauritzen, *Treatise Solid State Chem.*, **3** (1976).
(10) J. Maxfield and L. Mandelkern, *Macromolecules*, **10**, 1141 (1977).
(11) I. G. Voigt-Martin, E. W. Fischer, and L. Mandelkern, *J. Polym. Sci., Polym. Phys. Ed.*, **18**, 2347 (1980).
(12) P. J. Phillips and B. C. Edwards, *J. Polym. Sci., Polym. Phys. Ed.*, **13**, 1819 (1975).
(13) B. C. Edwards and P. J. Phillips, *J. Polym. Sci., Polym. Phys. Ed.*, **13**, 2117 (1975).
(14) E. N. Dalal and P. J. Phillips, *Macromolecules*, **16**, 1754 (1983).
(15) E. N. Dalal and P. J. Phillips, *Macromolecules*, **17**, 248 (1984).
(16) R. S. Stein and M. B. Rhodes, *J. Appl. Phys.*, **31**, 1873 (1960).
(17) R. van Antwerpen, Ph.D. Thesis, Delft, The Netherlands, 1971.
(18) K. L. Naylor and P. J. Phillips, *J. Polym. Sci., Polym. Phys. Ed.*, **21**, 2011 (1983).
(19) T. Davidson and B. Wunderlich, *J. Polym. Sci., Part A-2*, **7**, 377 (1969).
(20) N. Bekkedahl, *Trans. Faraday Soc.*, **35**, 483 (1939).
(21) S. Kavesh and J. M. Schultz, *J. Polym. Sci., Part A-2*, **8**, 243 (1970).
(22) R. H. Boyd, *Macromolecules* **17**, 903 (1984).
(23) J. D. Ferry, "Viscoelastic Properties of Polymers", 2nd ed., Wiley, New York, 1970.
(24) F. E. Karasz and L. D. Jones, *J. Phys. Chem.*, **71**, 2234 (1967).
(25) T. Ito and H. Marui, *Polym. J.*, **2**, 768 (1971).
(26) A. E. Woodward, personal communication.
(27) E. N. Dalal, Ph.D. Thesis, University of Utah, 1983.
(28) F. C. Frank and M. Tosi, *Proc. R. Soc. London, Ser. A*, **263**, 323 (1961).
(29) J. H. Magill, *Nature (London)*, **187**, 770 (1960).
(30) P. J. Phillips and Y. H. Kao, submitted for publication.
(31) G. S. Ross and L. J. Frolen, *J. Res. Natl. Bur. Stand, Sect. A* **79A**, 701 (1975).
(32) R. M. Gohil and P. J. Phillips, submitted for publication.
(33) S. Matsuoka, *J. Polym. Sci.*, **57**, 569 (1962).
(34) E. Baer and J. L. Kardos, *J. Polym. Sci., Part A*, **3**, 2827 (1965).

Brillouin and Raman Scattering Studies of Single-Crystal-Texture Polyethylene

Paul J. Phillips*† and Y. T. Jang

Department of Materials Science and Engineering, University of Utah, Salt Lake City, Utah 84112

Q. L. Liu and Chin-Hsien Wang

Department of Chemistry, University of Utah, Salt Lake City, Utah 84112

John F. Rabolt

IBM Research Laboratory, San Jose, California 95193. *Received August 24, 1984*

ABSTRACT: Single-crystal-texture polyethylene has been made from linear low-density polyethylene by solid-state extrusion followed by high-pressure annealing. X-ray studies show the material to have the following orientation functions: $f_c(200) = 0.983$, $f_c(020) = 0.976$, and $f_c(002) = 0.989$. The material is semicrystalline with a sheet structure. Raman studies show the lamellar thickness to be distributed about a 92-Å maximum. Brillouin scattering studies confirm the single-crystal texture of the material. Longitudinal and transverse modes could be studied with both high precision and polarization discrimination for the first time.

Introduction

It is well-known that orientation can be produced in crystalline polymers through mechanical deformation. Although uniaxially oriented materials have been studied thoroughly, biaxially oriented polymers, normally produced by drawing and rolling,[1,2] have received less attention. A special technique involving solid-state extrusion followed by high-pressure annealing was developed by Young and Bowden.[3] When this technique was applied to linear

† Present address: Department of Materials Science and Engineering, University of Tennessee, Knoxville, TN 37996-2200.

0024-9297/85/2218-1571$01.50/0

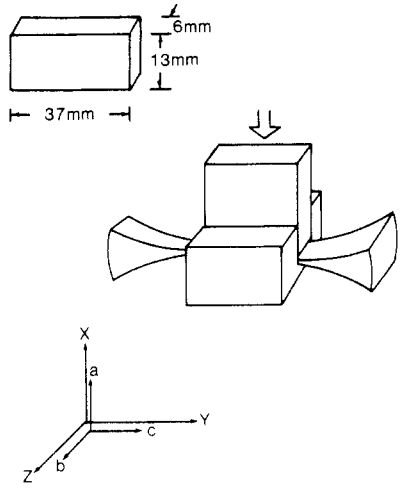

Figure 1. Schematic diagram of the slit extrusion process and principal specimen axes (*a*, *b*, and *c* refer to the unit vectors of the polyethylene crystal).

polyethylene, an orientation typical of single crystals was obtained in a polycrystalline material. This intriguing technique has not been applied to other polymeric systems, although the detailed morphology of single-crystal-texture linear polyethylene has now been elucidated.[4] In this contribution a modification of the technique for linear low-density polyethylene (LLDPE) will be described and the material characterized by a variety of means.

Since development of the multipass Fabry–Perot interferometer[5] Brillouin scattering has become increasingly useful[5-8] for studying the elastic properties of crystalline polymers. The technique has been applied to drawn and extruded polymers in the past. Different morphologies have been compared and their elastic constants related to parameters describing orientational ordering. In this paper the application of the Brillouin technique to a single-crystal-texture material will be described. The results are unique in that distinctive Brillouin spectra are obtained at different polarizations. The polarization discrimination achieved is similar to that attainable in a single crystal.

Experimental Section

Sample Preparation. Compression-molded sheets were produced by using a hot press at 150 °C and were air cooled to ambient temperature. These sheets were 37 mm in length, 6 mm in width, and 13 mm in height. This was achieved through the use of a window-shaped mold of these dimensions. The sample was then extruded at room temperature to 1.8 mm in height, without changing the length and width, using the device shown in Figure 1. The central portions of the extrudates were cut out and four pieces of them placed in the high-pressure bomb. A pressure of 4 kbar was then applied with the hot press, and the temperature was set at 185 °C for 1 h. The whole system was cooled to room temperature while still under pressure.

The temperature was chosen by employing a pressure coefficient of the melting point equal to 20 °C and an undercooling similar to that used by Young and Bowden,[3] allowing for the lower melting point of the LLDPE.

Sample Characterization. The crystallinity was estimated by differential scanning calorimetry. In order to do this the latent heat of fusion of an unoriented specimen whose crystallinity was already known from X-ray diffraction studies was first estimated by differential scanning calorimetry.

The orientation of the material was determined by X-ray diffraction. Samples were cut normal to the principal axes as defined in Figure 1. Laue photographs were then taken of the sections. The poles of the (200), (020), and (002) planes have their preferred orientations in the *X*, *Z*, and *Y* directions, respectively. The orientation functions were calculated from microdensitometer traces of the X-ray negatives by using the equation

$$f_c = (3\langle\cos^2\theta\rangle - 1)/2$$

where θ is the angle between the principal pole and its direction of preferred orientation. $\langle\cos^2\theta\rangle$ in each case was calculated as

$$\langle\cos^2\theta\rangle = (\sum\cos^2\theta_i I_i)/\sum I_i$$

where I_i is the intensity associated with the scattering angle θ_i.

The morphology was studied by scanning electron microscopy of samples fractured in liquid nitrogen. Samples were taken normal to all three principal axes.

Raman spectra were recorded by using a Jobin-Yvon HG-2S double monochromator equipped with an RCA 31034A-02 photomultiplier tube interfaced, via standard photon-counting electronics, to a Nicolet 1180 data system. The source of excitation was provided by the 488.0-nm line of a Spectra-Physics 165-08 argon ion laser. In general, the displayed spectra are the coaddition of multiple scans recorded at 1-cm^{-1} resolution at powers of 100–150 mW. Unless specifically noted the spectra have not been analog or digitally filtered.

Brillouin scattering was carried out by using single-mode laser radiation at ~488.0 nm as the excitation source. The scattered light at a specific polarization was selected with a Glann–Thomson polarizing prism. An interference filter transmitting only 488.0 ± 1.0 nm was used to block the Raman scattered light. A five-pass piezoelectrically scanned Fabry–Perot interferometer was employed to provide the spectral analysis of the scattered light. The overall instrumental finesse was greater than 60, and the free spectral range was 31.12 GHz.

Results

Structural Characterization. The crystallinity of single-crystal-texture LLDPE was found to be 80%. This is very much higher than that of an unoriented sample, where the value is 61%.

The orientation functions calculated as described in the previous section were $f_c(200) = 0.983$, $f_c(020) = 0.976$, and $f_c(002) = 0.989$. Values such as these were considered to be a clear indication of good orientation by Gray and Young.[10] As in the experiments of Young et al.[3,10] on linear polyethylene, there was no evidence of a monoclinic form in the specimen. The orientation function for the (200) reflection is considerably better than the best obtained for linear polyethylene by Gray and Young[10] of 0.972. The value for (002) is the same, the (020) value being marginally better (0.976 vs. 0.972). The orientability of the LLDPE was surprising since it had been expected that the lower initial crystallinity of LLDPE would make the process more difficult than in linear polyethylene. Our thickness reduction was 7.2 whereas the best value for linear polyethylene employed a thickness reduction of 25 at an elevated temperature.[10]

As occurs for linear polyethylene, fracture in the *YZ* plane was easiest. It can clearly be seen that the sample consists of large flakes (Figure 2). The sheet structure, which resembles that of mica, can be observed without magnification and can be seen if the sample is flicked with a finger when still cold. It produces a final structure similar to a pack of cards. Higher magnification studies (Figure 3) show that each sheet is in fact composed of subsheets with a thickness of approximately 5000 Å. Similar dimensions were reported by Young and Bowden[3] in their studies using transmission electron microscopy of replicas. During the fracture process the sheets break up into fibers. Studies of *YZ* planes show them to be flat and relatively smooth. The material is therefore made up of stacks of *YZ* plates, *Y* being the extrusion direction and *X* the compression direction. Since the molecular direction (*c*) is in the *Y* direction, any folded lamellar surfaces must be contained within the sheets.

Raman Scattering. The polarized low-frequency Raman spectra of the high-pressure annealed LLDPE is shown in Figure 4. The notation used to label each trace

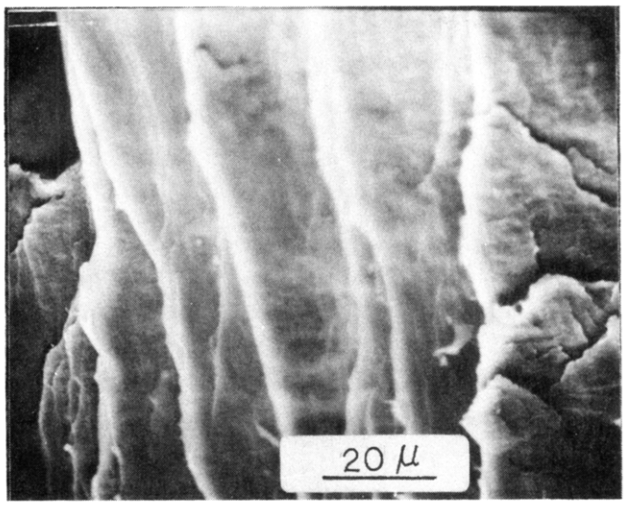

Figure 2. Scanning electron micrograph of a fractured specimen showing the flaky structure.

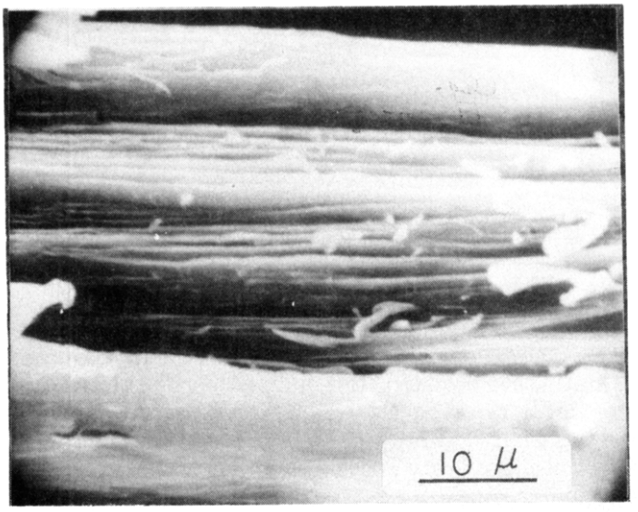

Figure 3. Scanning electron micrograph showing sheetlike substructure of the flakes.

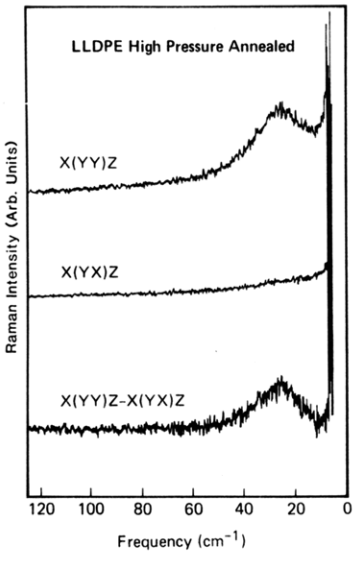

Figure 4. Polarized low-frequency Raman spectra of single-crystal-texture LLDPE.

is based on a scheme developed by Damen et al.[11] In this scheme the experiment is defined in terms of the laboratory coordinate system as

$$K_i(l_i l_s)K_s$$

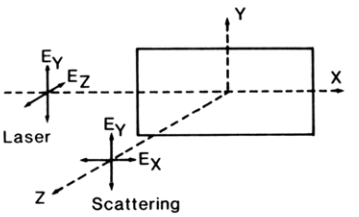

Figure 5. Schematic diagram of nomenclature used in polarized Raman studies.

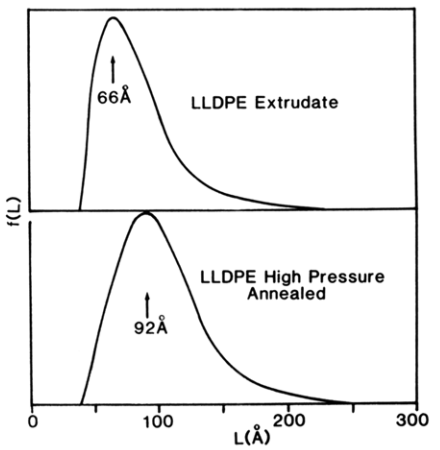

Figure 6. Stem length distributions of LLDPE specimens calculated from the elastic rod model.

where K_i is the direction of incident beam travel, l_i and l_s are the polarization of the incident and scattered light, respectively, and K_s is the direction in which the Raman scattered light is observed. In our notation the incoming beam is along the X axis, the scattered beam is along the Z axis, and the Y axis is perpendicular to the scattering plane (see Figure 5). For these experiments, the extrusion direction of the sample (Y of Figure 1) was placed parallel to the Y axis of Figure 5.

As seen by comparing the $X(YY)Z$ and $X(YX)Z$ polarizations, a high degree of orientation results upon extrusion through the slit die followed by high-pressure annealing. An indication of this is evident by the absence of the LAM in the $X(YX)Z$ spectrum. Since in PE the contribution to the intensity of the LAM band from a change in polarizability parallel to the chain axis is large, the appearance of the LAM in the $X(YY)Z$ spectrum will occur when high orientation of the chain axis parallel to Y is present. Poor orientation of the chain axes, on the other hand, would result in significant LAM intensity in the $X(YX)Z$ spectrum. Since this is not the case, the difference spectrum can be formed in order to correct the spectral background for the stray light characteristics of the double monochromator. This is shown in the lower panel of Figure 4. A recasting of the observed Raman intensity in terms of the change in polarizability with normal mode, I^α, which is directly relatable to molecular parameters, has been suggested by Snyder et al.[12] who found that removing the frequency and temperature effects on the Raman band intensity could influence the peak position of the LAM band depending on its bandwidth, greater shifts being observed for larger bandwidths. With an additional conversion of the Raman frequencies into chain lengths via the elastic rod model,[13] the profile of the LAM band can be recast into a stem length distribution function, $f(L)$, as shown in Figure 6. Both the extrudate (upper trace) and the high-pressure annealed LLDPE (lower trace) LAM profiles have been converted into their respective stem length distributions. Several interesting

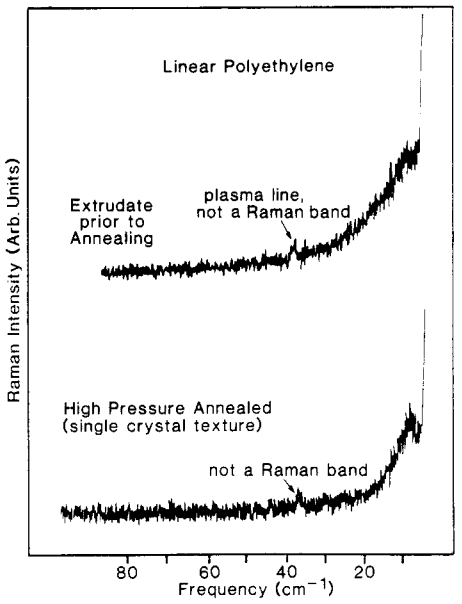

Figure 7. Polarized low-frequency Raman spectra of slit-extruded and single-crystal-texture linear polyethylene.

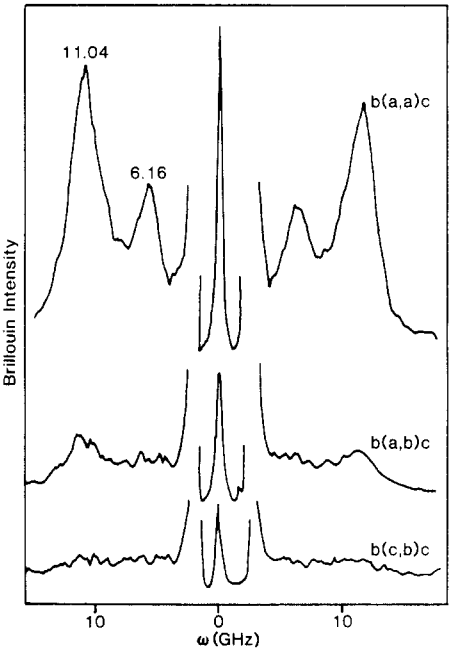

Figure 8. Brillouin spectra for the configurations indicated.

observations can be made regarding the maxima and the bandwidth of each distribution. The most probable stem length of 66 Å found for the extrudate shifts to 92 Å after high-pressure annealing, in accordance with the expected crystal-thickening process. What is surprising is that the increase in stem length was not larger since high-pressure annealing is known to produce extended chain (>2000 Å) crystals.[14] This most probably results because of the branch content of the LLDPE since the incorporation of long-chain branches within a lattice is energetically improbable and would thus limit the extended chain length.

It is also obvious from Figure 6 that the breadth of the stem length distribution also increases upon high-pressure annealing of the extrudate. Similar behavior has been observed by Koenig and Tabb[15] upon the annealing of single-crystal mats. It is possible that the broadening observed in the case of LLDPE may be caused by the nature and extent of branching found in the sample since, again, the high energy requirements of incorporating branches into the crystal could certainly influence the stem length distribution by skewing it toward the long-chain limit.

It can be seen that a fraction of the material has a lamellar thickness as high as 200 Å. In their studies of linear polyethylene Young and Bowden[3] used nitric acid etching followed by replication in an attempt to study the lamellar structure. The best electron micrographs obtained led to a value of 300 ± 50 Å in lamellae which were of irregular shape. Values obtained from small-angle X-ray scattering experiments led to similar estimates. These estimates were later confirmed by Burney and Groves,[4] who used the Kanig[16] technique of chlorosulfonic acid staining. We have prepared single-crystal-texture linear polyethylene using the Young and Bowden[3] technique. Extensive studies have not been carried out; however, Raman LAM spectra (Figure 7) clearly show a peak at ~6–8 cm^{-1} (which might shift by 0.5 cm^{-1} if corrected for frequency and temperature[12]). Stem lengths producing this band would be in the region of 350 Å. This figure correlates well with the aforementioned estimates of Young and Bowden[3] from electron micrographs and SAXS. Considerable confidence can therefore be placed in the stem lengths being derived for the LLDPE specimens, since our studies of HDPE correlate well with those of other workers.

Brillouin Scattering. The scattering geometry $K_i(l_i l_s)K_s$ described above in the Raman scattering section was also used to record the Brillouin spectra.

The Brillouin spectral intensity of an anisotropic medium is given by

$$I_{ij}(\mathbf{q}) = n_i^4 n_j^4 p_{ijkl} p_{ijk'l'} \langle |e_{ij}(\mathbf{q})|^2 \rangle \quad (1)$$

where the angular brackets denote the ensemble average; n_i and n_j are the refractive indices of refraction of the incident light propagating along the ith optical axis and the scattered light propagating along the jth optical axis, respectively. p_{ijkl} are Pockels photoelastic constant tensor components; $e_{kl}(\mathbf{q},t)$ are the spatial Fourier transform of the strain tensor components. $\mathbf{q}$ is the scattering vector whose magnitude is given by

$$q = \frac{2\pi}{\lambda}(n_i^2 + n_j^2 - 2n_i n_j \cos\theta) \quad (2)$$

where λ is the wavelength of the excitation laser in vacuo and θ is the scattering angle. The velocity of the acoustic waves is related to q by

$$v = 2\pi f_B / q \quad (3)$$

where f_B is the observed Brillouin frequency shift (in hertz).

Brillouin spectra have been obtained in various scattering configurations with the photon progagation vector $\mathbf{q}$ propagating in the a–b, a–c, and b–c planes are shown in Figures 8–10, respectively. See Figure 1 for correlation between Raman and Brillouin notations. The polarized spectra are prominent, whereas the spectral feature obtained in the depolarized scattering configuration is presumably due to slight polarization leakage. Note the distinctive difference in the Brillouin spectra obtained in various polarization selections. The clear polarization discrimination definitely shows that the sample has single-crystal texture.

The mean refractive index of polyethylene at room temperature is 1.524 and the birefringence of highly oriented polyethylene is about 10^{-3}. This is smaller than the experimental uncertainty in the present Brillouin frequency measurement. We can thus neglect the effect of birefringence in the sound velocity calculation. Assuming

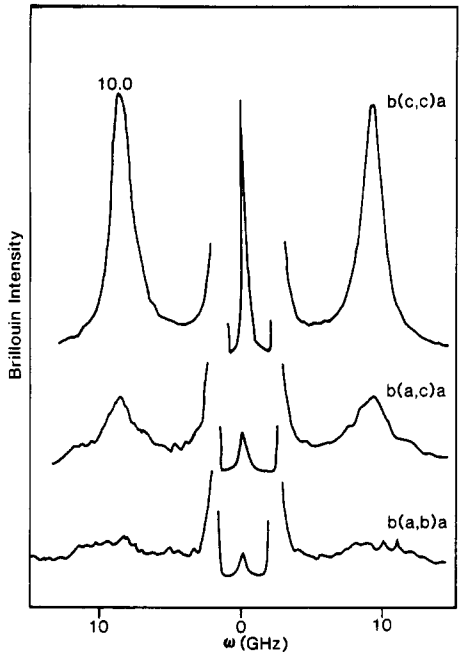

Figure 9. Brillouin spectra for the configurations indicated.

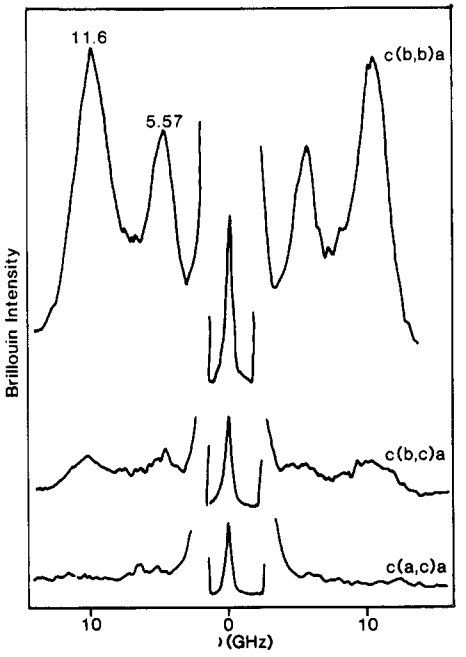

Figure 10. Brillouin spectra for the configurations indicated.

that $n_i = n_j = 1.524$, we have found that $q = 2.76 \times 10^5$ cm^{-1} for $\lambda = 488.0$ nm at $\theta = 90°$. The sound velocities (longitudinal, V_L; transverse, V_T) calculated by using the frequencies given in Figures 8–10 are given in Table I. In the $b(c,c)a$ spectrum, only the longitudinal acoustic peak is unresolved. On the other hand, both longitudinal and transverse peaks appear in the $c(b,b)a$ and $b(a,a)c$ spectra. The transverse velocity is about half of the longitudinal velocity in the present sample. Note that the longitudinal sound velocity detected in the $b(a,a)c$ geometry is marginally greater than that detected in the $a(b,b)c$ geometry, which is in turn greater than that in the $a(c,c)b$ geometry. Similarly, the transverse sound velocity obtained in $b(a,a)c$ is higher than that obtained in $a(b,b)c$. This result shows that the modulus exhibits a clear but modest anisotropy and is greater in the bc plane.

In this sample, the wavelength of the fluctuations probed by Brillouin scattering is 2275 Å (from π/q) so the technique did not detect the presence of lamellae outside the normal range of the LAM mode.[14]

Table I
Observed Acoustic Phonon Velocities in Various Scattering Geometries

scattering geom	$10^{-5}V_L$, cm/s	$10^{-5}V_T$, cm/s
$a(c,c)b = b(c,c)a$	2.28 ± 0.04	
$a(b,b)c = c(b,b)a$	2.45 ± 0.04	1.23 ± 0.04
$c(a,a)b = b(a,a)c$	2.51 ± 0.04	1.37 ± 0.04

Using eq 1 and assuming that the sample has orthorhombic symmetry, we find that the intensity of the $a(c,c)b$ spectrum is proportional to

$$\langle |p_{31}q_a u_a(\mathbf{q}) - p_{32}q_b u_b(\mathbf{q})|^2 \rangle$$

where q_a and q_b are the projection components of the $\mathbf{q}$ vector on the a and b axes. u_a and u_b are the projections of the particle displacement vector. p_{31} and p_{32} are Pockels photoelastic constants in the Voigt notation. Similarly, the $b(a,c)a$ spectral intensity is proportional to $\langle |p_{55}q_a u_c|^2 \rangle$, the $b(c,b)a$ intensity to $\langle |p_{44}q_b u_c|^2 \rangle$, and the $b(a,b)c$ intensity to $\langle |p_{66}(q_a u_b - q_b u_a)|^2 \rangle$. The fact that only the $b(c,c)a$ intensity is prominent shows that p_{31} and p_{32} are much larger than p_{44}, p_{55}, or p_{66}. The same conclusion is also obtained for the $a(b,b)c$ and $b(a,a)c$ spectra. Thus in the present sample, p_{12}, p_{13}, p_{31}, and p_{32} are much larger than p_{44}, p_{55}, or p_{66}. However, comparison of the intensity of the $b(c,c)a$, $a(b,b)c$, and $b(a,a)c$ spectra shows that the photoelastic coefficients p_{12}, p_{13}, p_{31}, and p_{32} have a similar magnitude.

Using Newton's equation from continuum mechanics and the orthorhombic symmetry for the elastic constant tensor, we find that the two Brillouin peaks observed in the $c(b,b)a$ scattering geometry are given by

$$\omega_\pm^2 = \frac{q^2}{4\rho}\{(c_{11} + c_{33} + 2c_{44}) \pm [(c_{33} - c_{11})^2 + 4(c_{13} + c_{44})^2]^{1/2}\} \quad (4)$$

the two peaks appearing in the $b(a,a)c$ geometry being given by

$$\omega_\pm^2 = \frac{q^2}{4\rho}\{(c_{22} + c_{33} + 2c_{44}) \pm [(c_{33} - c_{22})^2 + 4(c_{23} + c_{44})^2]^{1/2}\} \quad (5)$$

and the single peak appearing in the $b(c,c)a$ geometry being given by

$$\omega = \frac{q^2}{4\rho}\{(c_{11} + c_{22} + 2c_{44}) \pm [(c_{11} - c_{22})^2 + 4(c_{12} + c_{44})^2]^{1/2}\} \quad (6)$$

With only five frequency values for eight unknowns, the evaluation of each elastic constant is impossible. However, the fact that all three longitudinal velocities are different and two transverse velocities are also different indicates that $c_{11} \neq c_{22} \neq c_{33}$ and $c_{13} \neq c_{23}$ in the present sample. Using the back-scattering geometry, we have estimated that $c_{11} \leq 4.82 \times 10^{10}$ dyn/cm^2 and $c_{22} \leq 4.40 \times 10^{10}$ dyn/cm^2. Due to the sample size, we are unable to estimate c_{33}, but according to Table I and eq 4 and 5, we note that $c_{33} > c_{11} > c_{22}$.

Finally, it should be emphasized that the transverse peaks appearing in the $c(b,b)a$ and in the $b(c,c)a$ spectra are due to the transverse–longitudinal coupling. The na-

ture of these peaks is different from the transverse peak that is expected to appear in the depolarized $c(b,c)a$ or $b(a,c)a$ spectra but does not appear because of small p_{44} and p_{55} photoelastic constants. The present sample is mechanically anisotropic and the two transverse peaks are not degenerate. The transverse peak that is not observed is associated with the elastic constant c_{44}, and the transverse peaks that appear in the $c(b,b)a$ and in the $b(a,a)c$ spectra are associated with negative sign in eq 4 and 5. These frequencies become degenerate only when $c_{11} = c_{22} = c_{33}$ and $c_{13} = c_{23} = c_{12}$, as in this case the Cauchy relation $c_{11} - c_{12} = 2c_{44}$ applies.

Discussion

The results of X-ray diffraction studies, scanning electron microscopy, and inelastic (Raman) and quasi-elastic (Brillouin) light scattering studies lead to a definitive picture of the structure of single-crystal-texture polyethylene. The extrusion process leads to the production of a material consisting of stacked sheets. These sheets are approximately 5000 Å thick and are *bc* planes, the thinnest dimensions being aligned with the *a* axis. Orientation is such that all axes are misaligned by at most 5°, and the orientation is generally better than that achievable in linear polyethylene obtained by more extreme methods. The sheets are composed of oriented lamellae with a peak lamellar thickness of 92 Å but there is a distribution of thicknesses ranging as high as 250 Å. Since the crystallinity is 80% the average amorphous thickness separating the lamellae is of the order of 20 Å. Brillouin scattering did not detect the presence of thicker lamellae outside the normal range of Raman LAM studies. Since this linear low-density polyethylene, which is a copolymer of ethylene with octene, is essentially a blend of linear and short-branched molecules, the possibility of fractionation at the high annealing pressures was a distinct possibility. Bassett[17] has reported very clear evidence for fractionation according to branching in similar materials when crystallized above 4 kbar. Here, however, the material was not crystallized at pressure. It was annealed at a temperature just a few degrees below its melting point at 4 kbar. Annealing on its own, therefore, does not provide for fractionation. Rejection of branched molecules during the crystallization process is essential. Unlike linear polyethylene in single-crystal-texture form the lamellar thickness remains low. It is therefore determined by the branching frequency. Since the branches are too long to be incorporated into the polyethylene crystal, they must remain outside the lamellae. The fact that no really thick lamellae were observed means that the polymer had behaved as a compatible blend producing cocrystallized species. If there had been a substantial amount of segregation then a bimodal distribution of lamellar thicknesses would have resulted.

Acknowledgment. This research has been supported by the Army Research Office (P.J.P.) and the Polymers Program of The National Science Foundation (C.-H.W.).

References and Notes

(1) I. L. Hay and A. Keller, *J. Mater. Sci.*, **1**, 41 (1966).
(2) I. L. Hay and A. Keller, *J. Mater. Sci.*, **2**, 538 (1967).
(3) R. J. Young and P. B. Bowden, *J. Mater. Sci.*, **8**, 1177 (1973).
(4) S. G. Burney and G. W. Groves, *J. Mater. Sci.*, **12**, 1139 (1977).
(5) J. Sandercock, in "Light Scattering in Solids", Flammanion, Paris, 1971, pp 9–12.
(6) D. B. Cavanaugh and C. H. Wang, *J. Appl. Phys.*, **52**, 5998 (1981).
(7) D. B. Cavanaugh and C. H. Wang, *J. Appl. Phys.*, **53**, 2793 (1982).
(8) D. B. Cavanaugh and C. H. Wang, *J. Polym. Sci., Polym. Phys. Ed.*, **20**, 1647 (1982).
(9) J. J. Hermans, P. J. Hermans, D. Vermaas, and Q. Weidinger, *Recl. Trav. Chim. Pays-Bas.* **65**, 427 (1946).
(10) R. W. Gray and R. J. Young, *J. Mater. Sci.*, **9**, 521 (1974).
(11) T. C. Damen, S. P. S. Porto, and B. Tell, *Phys. Rev.*, **142**, 570 (1966).
(12) R. G. Snyder, S. J. Krause, and J. Scherer, *J. Polym. Sci., Polym. Phys. Ed.*, **16**, 1593 (1978).
(13) S. Mizushima and T. Shimanouchi, *J. Am. Chem. Soc.*, 71, 1320 (1949).
(14) J. F. Rabolt and C. H. Wang, *Macromolecules*, **16**, 1698 (1983).
(15) J. L. Koenig and D. L. Tabb, *J. Macromol. Sci., Phys.*, **B9**, 141 (1974).
(16) G. Kanig, *Kolloid Z. Z. Polym.* **251**, 782 (1973).
(17) D. C. Bassett, "Principles of Polymer Morphology", Cambridge University Press, 1981.

Investigation of Local Conformations of Polyelectrolytes in Aqueous Solution by Small-Angle X-ray Scattering. 1. Local Conformations of Poly(sodium acrylates)

Yoshio Muroga, Ichiro Noda,* and Mitsuru Nagasawa

Department of Synthetic Chemistry, Faculty of Engineering, Nagoya University, Furo-cho, Chikusa-ku, Nagoya 464, Japan. *Received October 1, 1984*

ABSTRACT: Local conformations of poly(sodium acrylates) in aqueous solutions with an added salt were studied by small-angle X-ray scattering measurements. It is concluded that the chain stiffness of poly(sodium acrylates) is not much affected by the electrostatic repulsions.

Introduction

The conformation of a polymer chain in solution is in general discussed on an assumption that the conformation is determined by two independent factors: (i) the local chain stiffness due to the steric hindrance between adjacent segments and (ii) the excluded volume effect working between segments far apart along a chain.

Analysis of the conformation of polyelectrolytes has also been carried out on the two-parameter assumption. The electrostatic repulsion between charged groups surely causes an excluded volume effect between segments located far apart along a chain. From light scattering study of poly(sodium acrylates), Kitano et al.[1] concluded that the conformation of a polyelectrolyte in solution is determined mainly by the excluded volume effect.

However, this conclusion does not deny a possibility that the electrostatic repulsion increases the stiffness of the polymer chain, since the magnitude of the scattering vector

0024-9297/85/2218-1576$01.50/0